Vol.38 高等学校化学学报 No.6
2017 年 6 月 CHEMICAL JOURNAL OF CHINESE UNIVERSITIES 982~989

doi: 10.7503/cjcu20160849

无针式静电纺丝喷头几何形状对电场分布规律的影响机理

王 巍, 强 威, 代红超
(天津工业大学电气工程与自动化学院, 天津市电工电能新技术重点实验室, 天津 300387)

摘要 根据射流的质量守恒、电荷守恒和动量守恒分析稳态射流的运动过程, 建立了控制方程组; 应用有限元分析软件 COMSOL Multiphysics 5.0 建立 3 种无针式喷头模型, 分析其外部电场的分布规律. 研究发现, 在由典型圆柱体喷头到增加辅助电极的阶梯轴喷头的几何形状变化过程中, 电场强度分布受两侧添加的辅助电极角度和增加回转体数量及回转体直径的影响, 通过设计, 电场被逐步优化. 对无针式静电纺丝装置的生产效率及纤维质量的提高具有重要意义.

关键词 静电纺丝; 喷头; 电场强度
中图分类号 O631; O441.4 **文献标志码** A

Impact Mechanism of Needleless Electrospinning Spinneret Geometry on Electric Field Distribution Regularities

WANG Wei*, QIANG Wei, DAI Hongchao
(*School of Electrical Engineering and Automation*,
Tianjin Key Laboratory of Advanced Technology of Electrical Engineering and Energy,
Tianjin Polytechnic University, *Tianjin* 300387, *China*)

Abstract In the needleless electrospinning technology, the distribution and the value of electric field at spinneret are the key factors that influence the electrospinning process and the formation of nanofibers. Different geometries of the spinneret directly affect the distribution of the external electric field. Therefore, it is of practical significance for the design and optimization of needleless electrospinning spinneret through the research on the distribution of electric field from the geometry. In this paper, governing equations had been set up to analyze movement process of steady-state jet from three aspects: mass conservation, charge conservation and momentum conservation. The finite element analysis(FEA) software COMSOL Multiphysics 5.0 is used to model three needleless electrospinning spinnerets and analyze the distribution of external electric field. It is found that during the evolution from the typical cylindrical spinneret to the stepped shaft one with the added auxiliary electrodes, the distribution of electric field is influenced by the angle of the auxiliary electrodes added on both sides, plus of the number and diameters of rotary parts. The electric field is optimized step by step through a series of designs. The research is very important to the improvement of production efficiency and nanofiber quality of the needleless electrospinning equipment.

Keywords Electrospinning; Spinneret; Electric field intensity

收稿日期: 2016-11-28. 网络出版日期: 2017-05-23.
基金项目: 国家科技支撑计划项目(批准号: 2014BAH03F01)资助.
联系人简介: 王 巍, 男, 博士, 教授, 博士生导师, 主要从事机电磁一体化理论及应用、汽车电子及测控、信号传输与处理研究.
E-mail: wangweibit@ tjpu.edu.cn

Electrospinning is the most effective and direct method for producing continuous nanofibers, and as-obtained nanofibers have excellent characteristics and wide applications[1]. However, the production efficiency of the single needle electrospinning equipment is generally extremely low; the maximum total mass of the nanofiber produced per hour is not more than 300 mg[2]. Although the production rate of the multi-needle electrospinning equipment is improved, the structure of the equipment is complex and the electric field interference between adjacent spinnerets is large[3]. The mutual interference can lead to the uneven distribution of the electric field, prompting unstable jet whipping at the needles and bringing difficulties to the nanofibers orientation collection, and then seriously affect the nanofibers quality[4]. In addition, there is a serious clogging problem no matter it is single needle or multi-needle electrospinning, greatly restricting the rapid development of electrospinning technology[5]. To solve these problems, researchers have proposed the needleless electrospinning equipment and carried out extensive researches[6—9]. In the needleless electrospinning equipment, when the electric field intensity exceeds the critical value, a large number of jets are formed directly from the open free fluid surface[10], which not only solves the problem of needle clogging, but also increases the production efficiency and nanofibers yield, as well as providing a feasible way for the industrialization of electrospinning[11].

At present, the needleless electrospinning technology has many methods, such as the global first electrospinning machine Nanospider developed by Czech Elmarco Corporation; it adopts a rotary cylinder to convert the solution attached on the cylinder into droplets, which form a Taylar cone and are drawn into a thin filament under the action of electric field force[12,13]. Huang *et al.*[14] designed two kinds of rotary cylindrical spinne-rets, one kind of spinneret surface has a lot of protrusions and another spiuneret surface is smooth. Niu *et al.*[2] found that the electric field intensity around the spiral was high and uniform, resulting in good nanofiber quality and great yield when using a conical spiral wire coil spinneret. Throughout these studies, the formation and trajectory of the jet in the fiber-forming process of the polymer solution depends on the distribution of the electric field intensity. For needleless electrospinning equipment, the spinneret geometry is a direct factor on the distribution of the external electric field intensity when the same voltage is applied. Therefore, the design of the spinneret geometry has practical significance to optimize the distribution of electric field intensity in the process of needleless electrospinning.

In this paper, the authors implement researches on the distribution of the external electric field intensity of three spinnerets with different geometries under the same voltage, including the cylinder, the cylinder with auxiliary electrodes and the stepped shaft with auxiliary electrodes. The FEA software COMSOL Multiphysics 5.0 is used to analyze and compare the electric field of the three models, with the aim to provide an effective way to optimize the electrostatic field and provide effective reference for further researches and designs of the needleless electrospinning spinneret.

1 Dynamic Balance Analysis of Steady-State Jet

1.1 Mass Conservation

Take the electrostatic spinning jet micro elements as shown in Fig.1. According to the law of conservation of mass, the mass of fluid flowing in the micro element is equal to that flowing out the micro element in the unit time. Namely, $\pi r_1^2 v_1 \rho_1 = \pi r_2^2 v_2 \rho_2$. Unit jet flow is assumed to be Q, therefore:

$$Q = \pi r^2 v \rho \tag{1}$$

Whereas, r is jet micro element's radius, v is jet velocity, and ρ is jet density.

1.2 Charge Conservation

When jet moves in the electric field, the formed current consists of three sections[15,16]: ohmic conductor

current, surface current formed by the jet movement, current formed by polarization charge, which is generated by external electric field driving polymer solution molecular orientation along the direction of electric field.

1.2.1 Ohmic Conductor Current The anions and cations ionized in the polymer solution are shifted directionally under the action of the electric field; the anions are generally concentrated inside the jet, and the cations are concentrated on the surface. The charge distribution inside the jet is similar to that of the conducting metal, conforming to the Ohm law. Therefore:

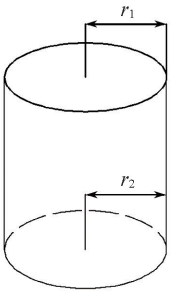

Fig.1 Schematic diagram of fluid mass conservation

$$I_1 = k\pi r^2 E \tag{2}$$

Whereas, k is the conductivity of the charged fluid, r is the radius of the micro fluidic element, and E is the electric field intensity.

1.2.2 Surface Current The charge carried by cations on the surface of polymer solution forms current because of the jet motion. Because the electric quantity passing through the cross section is current, the surface current is:

$$I_2 = 2\pi r v \sigma \tag{3}$$

Whereas, σ is the surface charge density, r is the radius of the jet micro element, and v the jet speed.

1.2.3 Polarization Current To polymer solution in the external field, each molecule has some induced electric dipoles[17]; the moment of external electric field on the electric dipoles let each molecule in directional alignment, resulting in positive and negative charges on the two surfaces, which are perpendicular to the polymer solution and the external electric field. In the process, positive and negative charges produce displacement to form polarization current. According to Curie Weiss law, the degree of polarization of the molecule is inversely proportional to the temperature. Macroscopically, an additional field is generated due to generation of polarized charges, namely the polarization charge electric field. The electric field of the polarized charges acts on the original electric field, so that each point's field intensity in the space is rearranged:

$$\vec{E} = \vec{E}_1 + \vec{E}_2 \tag{4}$$

whereas, $\vec{E}$ is the total electric field at any point in the space, $\vec{E}_1$ is a free charge field, and $\vec{E}_2$ is the polarization charge electric field. According to Gauss's law:

$$\vec{D} = \varepsilon_0 \vec{E} + \vec{P} \tag{5}$$

When the electric field $\vec{E}$ in the dielectric is not strong, the electrode intensity of the isotropic dielectric is proportional to $\vec{E}$, with the same direction:

$$\vec{P} = \varepsilon_0(\varepsilon_r - 1)\vec{E} \tag{6}$$

The relationship between the electric displacement vector and the electric field intensity can be expressed as:

$$\vec{D} = \varepsilon_0 \varepsilon_r \vec{E} \tag{7}$$

From the above equation, the polarization current generated by polarized charges can be expressed as follows:

$$I_3 = 2\pi r \varepsilon_0 \varepsilon_r E v \tag{8}$$

In summary, a partial differential equation can be expressed as follows according to the law of conservation of electric charge:

$$\frac{\partial}{\partial z}[2\pi r v(\sigma + \varepsilon_0 \varepsilon_r E) + \pi r^2 k E] + \frac{\partial}{\partial t}[2\pi r(\sigma + \varepsilon_0 \varepsilon_r E)] = 0 \tag{9}$$

Whereas, $\vec{D}$ is the electric displacement vector, $\vec{P}$ is the electric polarization intensity; ε_0 is the vacuum dielectric constant, and ε_r is the relative dielectric constant of dielectric.

1.3 Momentum Conservation

In the process of electrospinning, the motion jet micro element is affected by the electric field force, molecular polarization force, non Newtonian viscous resistance, liquid surface tension and gravity simultaneously. The electrospinning process is shown as Fig.2.

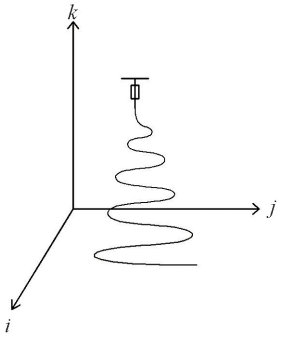

Fig.2 Scheme diagram of electrospinning process

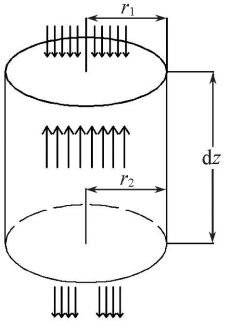

Fig.3 Schematic analysis of micro element visco-us resistance

1.3.1 Electric Field Force The electric field strength generated by the high voltage static electricity applied in the electrospinning process is assumed as $\vec{E}$, the electric field force on micro elements can be expressed as follows:

$$\vec{F}_1 = (2\pi r\sigma dz + k\pi r^2 E)\vec{E} \tag{10}$$

Whereas, σ is the surface charge density of the jet microelement.

1.3.2 Non-Newtonian Fluid Viscous Resistance The taken micro element is shown in Fig.3. It is assumed the stress exerted on some surface element of the micro element is τ and the internal pressure is T [18,19]. There is $\tau' = \tau - T$ (taking the direction of gravity as the positive direction). Apply Taylor series expansion:

$$\mathrm{d}\tau' = (\frac{\mathrm{d}\vec{\tau}}{\mathrm{d}z} - \frac{\mathrm{d}\vec{T}}{\mathrm{d}z})\mathrm{d}z \tag{11}$$

Thus, the viscous resistance of the jet element:

$$\vec{F}_2 = \pi r^2(\frac{\mathrm{d}\vec{\tau}}{\mathrm{d}z} - \frac{\mathrm{d}\vec{T}}{\mathrm{d}z})\mathrm{d}z \tag{12}$$

1.3.3 Surface Tension In order to facilitate the analysis of the surface tension, the moving jet is discretized into a finite numbers of infinitesimal spheres with a radius of a (a is infinitesimal). According to the formula of surface tension $F = \alpha l$ [20]:

$$F_3 = 2\pi a\alpha(\sin\theta + \cos\theta) \tag{13}$$

Because thesphere curvature $k_i = 1/a$, it can be written as:

$$F_3 = 2\pi a^2 k_i\alpha(\sin\theta + \cos\theta) \tag{14}$$

The surface tension of the jet micro element is:

$$\vec{F}_3 = \frac{2\pi a^2 k_i\alpha}{(x_i^{\,2} + y_i^{\,2})^{1/2}}[\vec{i}\,|x|\mathrm{sign}(x_i) + \vec{j}\,|y|\mathrm{sign}(y_i)] \tag{15}$$

Whereas, (x_i, y_j, z_j) is an arbitrary micro element's center coordinates, and θ *is* the angle between the sphere center and coordinate origin.

1.3.4 Molecular Polarizability The relationship between the amount of polarization charge and the electric displacement vector [Formula (7)] can be deduced: the amount of polarization charge generated is proportional to the electric field gradient, namely:

$$q_e = \varepsilon_0\varepsilon_r \nabla\vec{E} \tag{16}$$

Thus, the polarization force is:

$$\vec{F}_4 = \varepsilon_0 \varepsilon_r \nabla \vec{E} \cdot \vec{E} \tag{17}$$

1.3.5 Gravity The micro element is still shown in Fig.3. It is assumed the polymer solution is distributed evenly after mixing, and the density is ρ, so gravity exerting on the micro body is:

$$\vec{F}_5 = \pi r^2 \rho g dz \tag{18}$$

According to Newton's Second Law of Motion, the above contents can be summarized as follows:

$$\pi r^2 \rho dz \frac{d\vec{v}}{dt} = (2\pi r\sigma dz + k\pi r^2 E)\vec{E} + \pi r^2 \rho g dz + \frac{2\pi a^2 k_i \alpha}{(x_i^2 + y_i^2)^{1/2}}[\vec{i}|x|\text{sign}(x_i) + \vec{j}|y|\text{sign}(y_i)] +$$

$$\varepsilon_0 \varepsilon_r \nabla \vec{E} \cdot \vec{E} + \pi r^2 (\frac{d\vec{\tau}}{dz} - \frac{d\vec{T}}{dz}) dz \tag{19}$$

Formula(19) is the motion differential equation of the jet micro element.

The analysis of the electrospinning process is actually the analysis of the motion of the polymer solution under multiple fields' actions, including high voltage electrostatic field, force field and flow field. The high voltage electrostatic field is the main factor that affects the trajectory of the jet, the diameter of the fiber, the uniformity and quality of the fiber. Therefore, it is crucial to control the electric field environment with directed attention.

2 Electric Field Simulation

2.1 Typical Cylindrical Spinneret

A typical needleless electrospinning model is established with SOLIDWORKS, as shown in Fig.4. The model consists of a rotary cylinder spinneret, a polymer solution bath, a collector and a high voltage power supply. One part of the cylindrical spinneret shall be immersed in the polymer solution bath. During the normal operation of the model, the polymer solution in the bath will be attached to the spinneret when the spinneret is rotating. The polymer solution on the top surface of the cylinder will form a Taylor cone, thus forming jet and being drawn into nanofibers to fall on the collector when high voltage is applied between the spinneret and the collector. We set the cylindrical spinneret 16 cm in length, 2 cm in diameter; the polymer solution bath 20 cm in length, 10 cm in width, 2 cm in height; the collector 30 cm in length, 20 cm in width, 2 mm in height and collection distance 13 cm. Voltage of 60 kV is applied between the cylindrical spinneret and the collector. A 2D model is built with COMSOL Multiphysics 5.0.

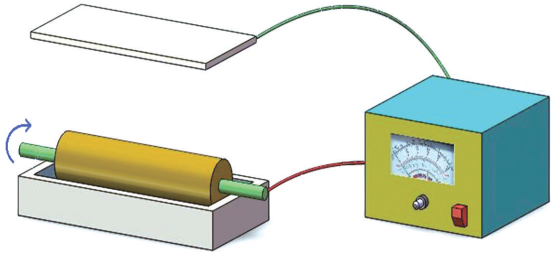

Fig.4 Schematic diagram of needleless electrosp-inning model

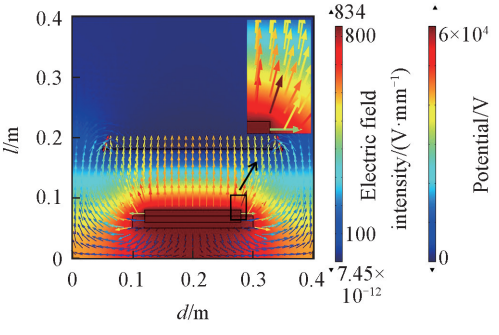

Fig.5 Surface arrow diagram of the electric field distribution of the cylinder spinneret

Fig.5 shows the vector arrow diagram of the electric field intensity distribution. The change trends of the electric field intensity at 0, 1, 2, 3 and 4 mm of cylindrical upper surface are observed, as shown in Fig.6. Obviously, the electric field intensity distribution is not uniform when the cylindrical spinneret is used. The maximum intensity 1500 V/mm appears at both ends of the cylinder while it is only about 700 V/mm in the middle area of the cylinder. With the increase of the cross-section position, the electric field intensity at both ends of the cylinder decreases gradually, but that in the middle almost does not change.

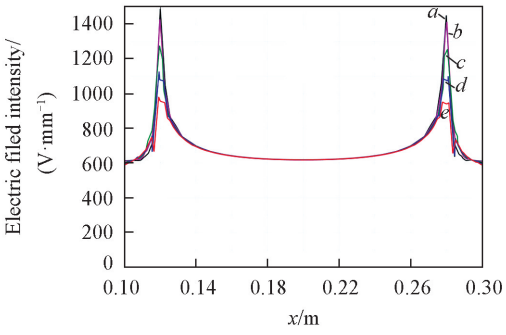

Fig.6　Distribution of the field intensity on the surface of the cylinder head at different heights in the *x*-axis direction

Height/mm: *a*. 0; *b*. 1; *c*. 2; *d*. 3; *e*. 4.

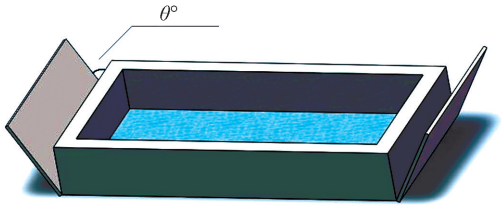

Fig.7　Schematic diagram of polymer solution bath with the auxiliary electrodes

2.2　Cylindrical Spinneret with Auxiliary Electrodes

In view of the above problems, whether some methods can be used to reduce peak values of the electric field intensity at both ends of the cylinder or increase the value in the middle, so that a uniform electric field distribution on the surface of the cylinder can be realized.

In this paper, the method, adding auxiliary electrodes on both sides of the polymer solution bath, is used to influence the electric field intensity at both ends of the cylinder, as shown in Fig. 7. Set the auxiliary electrodes 10 cm in length, 3 cm in width and 1 cm in height. The auxiliary electrodes are connected to the bottom of the polymer solution bath. The peak values of the electric field intensity at both ends of the cylinder are analyzed when θ = 0°, 30°, 45°, 60°, 90°. In the modeling, the part of the cylinder immersed in the solution is below its axis. When the cylinder diameter is 2 cm, the part of the spinneret exposed to the air is larger than 1 cm. The height of the solution bath is set to 2 cm, so the distance from the bottom of the bath to the cylindrical upper surface is at least 3 cm. The auxiliary electrodes are perpendicular to the horizon when θ=0°, and its maximum height is 3 cm, which is still smaller than the height of the upper surface of the cylinder. The electric field tip effect at both ends of the cylinder can be prevented from being transferred to the auxiliary electrodes to avoid the process of electrospinning being affected.

The voltage of 60 kV is applied between the spinneret and the auxiliary electrodes and the value of θ is changed. It is found that the electric field peak at the both ends of the typical cylinder spinneret with the auxiliary electrodes is obviously weakened. The smaller the angle, the stronger weaken ability will be. The peak value is 900 V/mm when θ = 0°. The value is significantly lowered for the peak of 1500 V/mm when the auxiliary electrodes are not added. Fig.8 shows the distribution of the electric field intensity in the *x*-axis direction at 1 mm on the upper surface of the cylinder. It can be seen from the Fig.8 that the electric field intensity in the middle region is about 600—700 V/mm, which is close to aforementioned 700 V/mm. The simulation process shows that the addition of the auxiliary electrodes has obvious effect on the electric field at both ends of the cylinder and has little effect on that in the middle region.

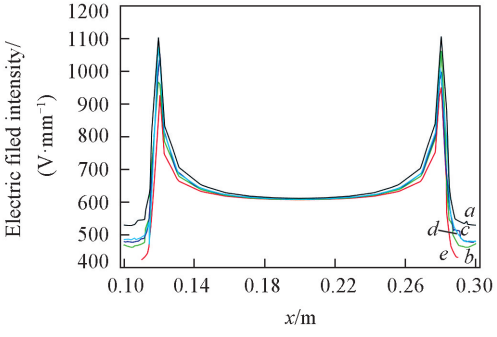

Fig.8　Electric field intensity distribution in the *x*-axis direction at 1 mm on the upper surface of the cylinder spinneret

θ/(°): *a*. 0; *b*. 30; *c*. 45; *d*. 60; *e*. 90.

2.3　Stepped Shaft Spinneret with Auxiliary Electrodes

We add the auxiliary electrodes on both sides of the polymer solution bath in the above, which changes

the electric field peak values at both ends of the cylinder, but has little effect on the electric field in the middle region. Therefore, we propose the idea to use the stepped shaft to change the electric field intensity in the middle region of the cylinder.

Fig.9(A — D) show the evolution from the typical cylinder to the stepped shaft built with SOLIDWORKS. In the modeling process, the influences of the number and diameters of rotary parts on the stepped shaft on its external electric field intensity distribution are studied.

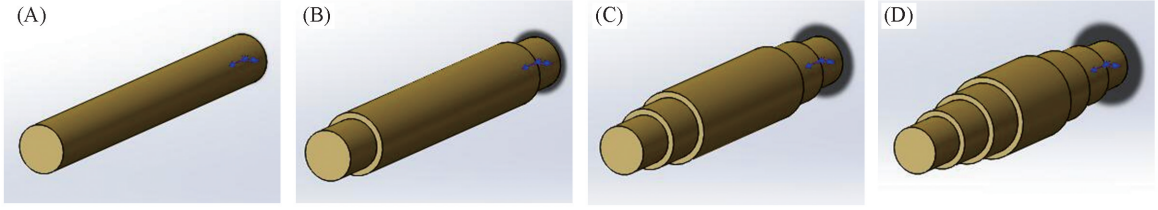

Fig.9 Evolution schematic diagram of the spinneret from typical cylinder to stepped shaft

2.3.1 Increase the Number of Rotary Parts The main diameter of the stepped shaft is 2 cm, with three rotary parts of diameter(ϕ) of 2.2, 2.4 and 2.6 cm, respectively, are added. The thickness variation of the rotary parts is the same, as shown in Fig.9(D). In the modeling, the polymer solution bath with auxiliary electrodes is still used, and voltage of 60 kV is applied to the spinneret and the auxiliary electrodes. The electric field intensity distribution is shown in Fig.10. Compare Fig.10 with Fig.5, Fig.6 and Fig.8, it can be obviously seen that there will be two peak values in the lower region of the middle electric field once one rotary part is added. Thus, the peak values in middle region will become more intensive with the increase of the number of the rotary parts. But a number of peak values in the middle region are still about 700 V/mm, which is similar to the electric field in the middle region shown in Fig.8 and no obvious improvement is achieved.

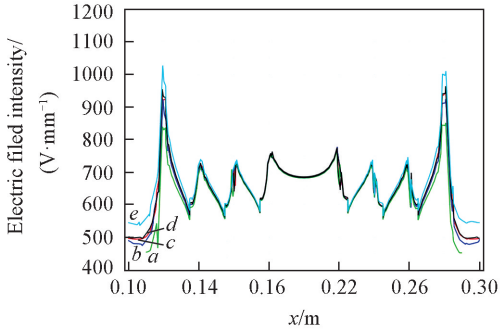

Fig.10 Electric field intensity distribution in the *x*-axis direction at 1 mm on the upper surface of the stepped shaft

θ/(°): *a*. 0; *b*. 30; *c*. 45; *d*. 60; *e*. 90.

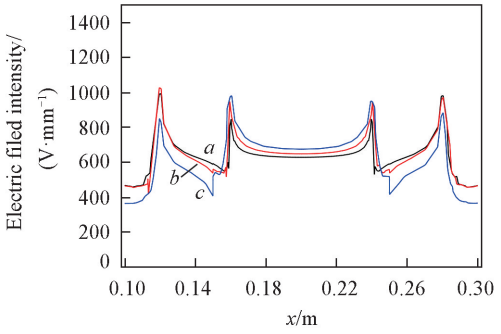

Fig.11 Electric field intensity distribution in the *x*-axis direction at 1 mm on the upper surface of the stepped shaft(θ=30°)

Length/cm: *a*. 2.4; *b*. 2.8; *c*. 3.2.

2.3.2 Change the Outer Diameter of Rotary Parts The main diameter of the stepped shaft is still 2 cm and a rotary part is added to the outside. The outer diameter of the rotary part is set to ϕ=2.4, 2.8, 3.6 cm, respectively. The inner diameter remains unchanged, that is, the thickness of the rotary part is changed. Through modeling and analysis of the three cases, it is shown that, the electric field in the middle region is improved significantly when the outer diameter of the rotary part is increased. The outer diameter ϕ=2.8 cm of the rotary part is better than other two cases, as shown Fig.11.

At this time, the electric field intensity is about 1000 V/mm at both ends of the stepped shaft and about 950 V/mm in the middle region. The adjacent peak values are approximately uniform. Through comparison with Fig.9, it not only satisfies the peak value in the middle region, the peak value is also increased, and better effect is realized.

3 Conclusions

This paper analyzes the influence of contents (including the properties of the polymer solution, the working electric field of the spinning process and the rheology of the polymer solution) on the electrospinning process theoretically. Moreover, the control equations of the steady-state jet are established, including jet's conservation of mass, conservation of charge and conservation of momentum. The FEA software COMSOL Multiphysics 5.0 is used to model the electric field distribution on the needleless electrospinning. It is found that peak values of the electric field intensity of the typical cylindrical spinneret appear at both ends. The peak values of the electric field intensity of the cylinder spinneret at both ends are weakened significantly, but the middle region is almost unchanged when the auxiliary electrodes with angle θ is added at both sides of the polymer solution bath. The electric field distribution of the middle region can be changed obviously by the stepped shaft spinneret with the auxiliary electrodes; however, it is influenced by the outer diameter of the rotary part. The evolution from the typical cylindrical spinneret to the stepped shaft spinneret with auxiliary electrodes, the electric field is optimized step by step. The research not only has a guiding role in the optimal design of needleless electrospinning spinnerets, but also has important significance for improving production efficiency and nanofiber quality of needleless electrospinning spinnerets.

This paper is supported by the National Key Technology R & D Program of China (No.2014BAH03F01).

References

[1] Bhardwaj N., *Biotechnology Advances*, **2010**, *28*(3), 325347
[2] Wang X., Niu H. T., Lin T., Wang X. G., *Polymer Engineering and Science*, **2009**, *49*(8), 1582—1586
[3] Deng Y. A., Huang X. H., Chen J. J., Wu Q. X., *Journal of Textile Research*, **2011**, *32*(8), 17—20
[4] Zhang Z. R., Liu Y. B., Ma Y., *Advanced Textile Technology*, **2012**, *28*(6), 9—11
[5] Xie K., Song Q. S., Deng D. P., Liu Y., *Engineering Plastics Application*, **2014**, *46*(6), 117—121
[6] Yarin A. L., Zussman E., *Polymer*, **2004**, *45*, 2977—2980
[7] Lu B., Wang Y., Liu Y., Duan H., Zhou J., Wang Y., Li X., Wang W., Lan W., Xie E., *Small*, **2010**, *6*(15), 1612—1616
[8] Holopainen J., Penttinen T., Santala E., Ritala M., *Nanotechnology*, **2015**, *26*(26), 025301
[9] Dosunmu O. O., Chase G. G., Kataphinan V., Reneker D. H., *Nanotechnology*, **2006**, *17*(4), 1123—1127
[10] Lukas D., Sarkar A., Pokorny P., *Journal of Applied Physics*, **2008**, *103*(8), 084309
[11] Hao M. L., Guo J. S., *China Textile Leader*, **2013**, (1), 58—60
[12] Molnár K., Kostakova E., Meszaros L., *Express Polymer Letters*, **2014**, *8*(1), 62—72
[13] Jirsak O., Kalinova K., Stranska D., *Vdi Berichte*, **2006**, *1940*, 41—44
[14] Huang X. P., Wu D., Zhu Y., Sun D., *IEEE-NANO IEEE Conference on Nanotechnology*, **2007**, *45*(9), 823—826
[15] He J. H., Wan Y. Q., Yu J. Y., *International Journal of Nonlinear Sciences and Numerical Simulation*, **2004**, *5*(3), 243—252
[16] He J. H., *Polymer*, **2004**, *45*, 9067—9070
[17] Lewowski T., *American Journal of Physics*, **1998**, *66*(9), 833—835
[18] Spivak A. F., Dzenis Y. A., *Applied Physics Letters*, **1998**, *73*(21), 3067—3069
[19] Tiwari D. K., Awasthi M. U., Agrawal G. S., *International Journal of Applied Mechanics*, **2012**, *4*(3), 1250027
[20] Reneker D. H., Yarin A. L., Fong H., Koombhongse S., *Journal of Applied Physics*, **2000**, *87*(9), 4531—454

(Ed.: W, Z)